Supporting Information for Observation of Coexistence of Yu-Shiba-Rusinov States and Spin-Flip Excitations

Shawulienu Kezilebieke,[†] Rok Žitko,[‡,¶] Marc Dvorak,[†] Teemu Ojanen,[†,§] and Peter Liljeroth[*,†]

[†]*Department of Applied Physics, Aalto University School of Science, 00076 Aalto, Finland*

[‡]*Jožef Stefan Institute, Jamova 39, SI-1001 Ljubljana, Slovenia*

[¶]*Faculty of Mathematics and Physics, University of Ljubljana, Jadranska 19, SI-1000 Ljubljana, Slovenia*

[§]*Computational Physics Laboratory, Physics Unit, Faculty of Engineering and Natural Sciences, Tampere University, P.O. Box 692, FI-33014 Tampere, Finland*

E-mail: Email:peter.liljeroth@aalto.fi

Additional experimental details

Sample preparation and subsequent STM experiments were carried out in an ultrahigh vacuum system with a base pressure of $\sim 10^{-10}$ mbar. The $2H$–$NbSe_2$ single crystal (HQ Graphene, the Netherlands) was cleaved in situ by attaching a tape to the crystal surface and pulling the tape in vacuum in the load-lock chamber using the sample manipulator. MPc molecules (Sigma-Aldrich) were deposited from an effusion cell held at 390°C onto a freshly cleaved $NbSe_2$ at room temperature.

After the MPc deposition, the sample was inserted into the low-temperature STM (Unisoku USM-1300) and all subsequent experiments were performed at $T = 4.2$ K. STM images were taken in the constant-current mode. $\mathrm{d}I/\mathrm{d}V$ spectra were recorded by standard lock-in detection while sweeping the sample bias in an open feedback loop configuration, with a peak-to-peak bias modulation of $50 - 100$ μV at a frequency of 709 Hz. The procedure for acquiring a spectrum was as follows: the tip was moved over the molecule at the imaging parameters (e.g. $V = 0.6$ V and $I = 5$ pA), the tip-sample distance was reduced by changing the setpoint to e.g. 200 pA at 100 mV. Finally, after disconnecting the feedback at the beginning the $\mathrm{d}I/\mathrm{d}V$ spectrum, the tip-sample distance was decreased by a further $50 - 100$ pm (z_{offset}) to increase the signal to noise ratio. The detailed numbers are given in the figure captions.

The $NbSe_2$ tip was prepared by indenting the tip into the $NbSe_2$ surface by a few nanometers while applying a voltage of 10 V. Manipulation of the MPc was carried out by placing the tip above the centre of the molecule with a bias voltage of 0.1 V and the current was increased to 1 nA with the feedback engaged. The tip was then dragged towards the desired location.

Geometries and spin densities from DFT calculations

Density functional theory calculations were performed with the FHI-AIMS computational package[1,2] and the PBE generalized gradient approximation for the exchange-correlation functional.[3] We used the standard "light" numerical settings and basis sets of numeric atomic-centered orbitals tested and recommended by FHI-AIMS. Periodic $NbSe_2$ supercells were sampled with a 2×2 k-point grid centred on the Γ point. Van der Waals interactions were included by the post-SCF Tkatchenko-Scheffler correction.[4] Before computing the electronic structure, all atomic forces were relaxed to < 0.01 eV/Å.

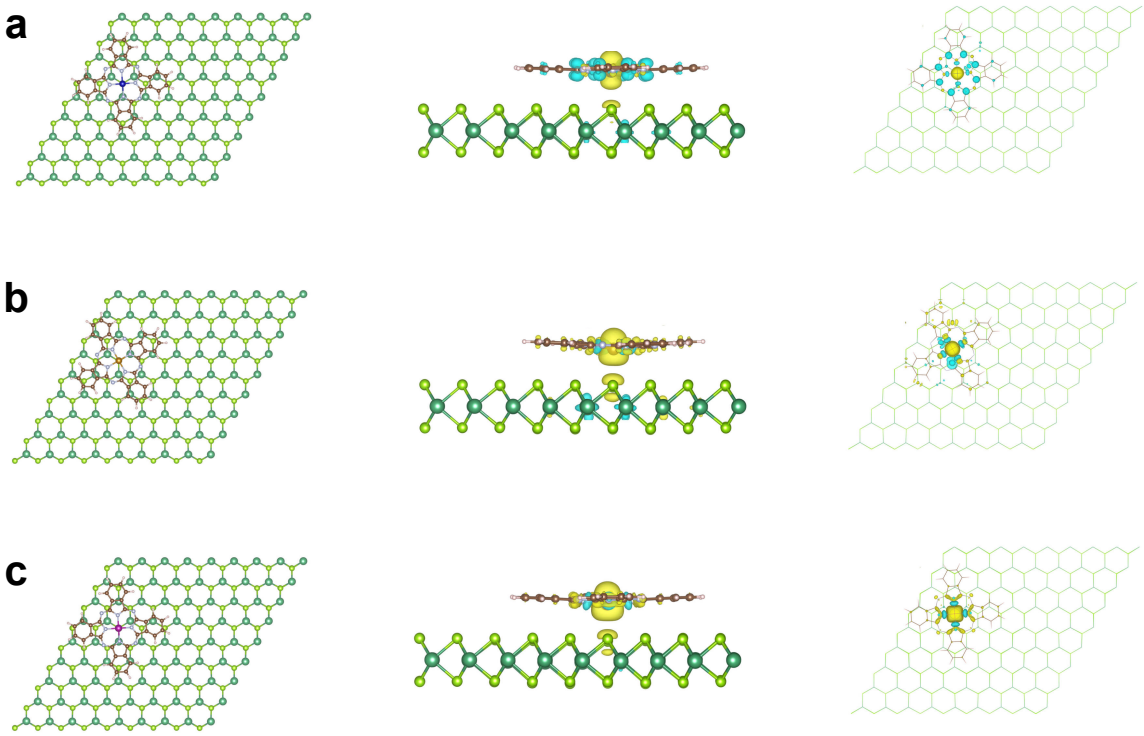

Figure S1: (a,b,c) Results for CoPc (a), FePc (b), and MnPc (c) computed with density functional theory (DFT).[1,2] The total computed spins for the systems are $S = 0.41$, $S = 1.22$, and $S = 1.72$, respectively. The localized metal atom-projected (Co, Fe, or Mn) spins are $S = 0.49$, $S = 1.10$, and $S = 1.70$, respectively. The localized atom-projected spins differ by < 0.1 compared to their gas phase counterparts with the same DFT parameters and numerical settings.

Experiments on FePc in external magnetic field

We can verify that the observed transitions in FePc do indeed correspond to inelastic spin excitations by acquiring $\mathrm{d}I/\mathrm{d}V$ spectra at different magnetic (B) field strengths aligned perpendicular to the sample surface. The energies of the first and second feature change with the external field, demonstrating that these are spin excitations (see Fig. S2). The

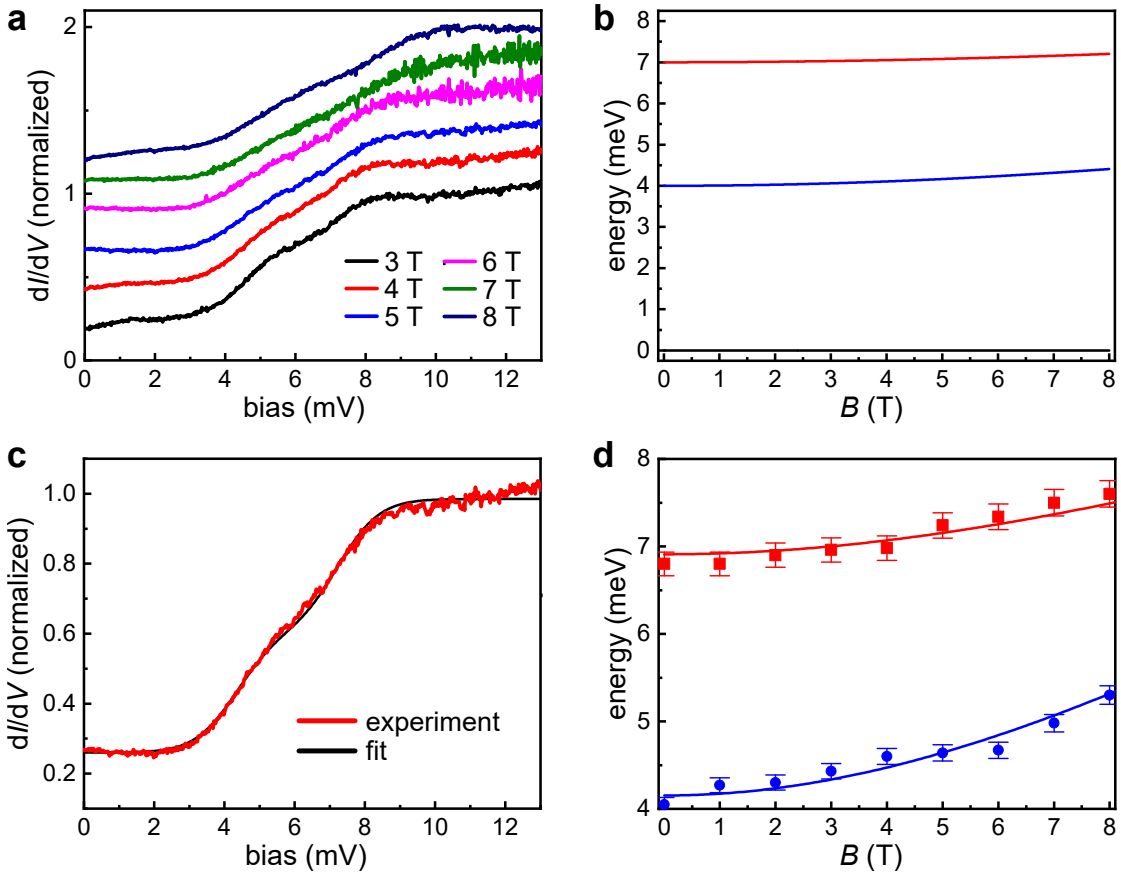

Figure S2: Spin-flip excitations in FePc under external magnetic field. (a) $\mathrm{d}I/\mathrm{d}V$ spectra of FePc taken as a function of B_z (3 - 8 T, perpendicular to the sample surface). Each spectrum was acquired directly above the central Fe atom of the FePc. The spectra are vertically offset for clarity (set-point conditions: 20 mV / 1 nA). (b) Schematic level diagram for an $S = 1$ system with $g = 2$, $D = 5$ meV and $E = 1$ meV. Due to the selection rule $m_S = \pm 1$, there are two allowed transitions from the ground state. (c) $\mathrm{d}I/\mathrm{d}V$ spectrum measured under an external field of 5 T showing the splitting of the inelastic spin excitation due to the presence of transverse magnetic anisotropy term E. The black line represents the fit of the spectra.[5] (d) Spin-flip energies as a function of the external magnetic field. From the fit, we obtain $g = 3.6$, $D = 5.5$ meV, and $E = 1.4$ meV.

zero-field splittings (ZFS) are well described by the following spin Hamiltonian:

$$H_{\text{eff}} = DS_z^2 + E(S_x^2 - S_y^2)$$

where D is the axial ZFS constant to determine the magnetic anisotropy, E is the transverse anisotropy, and S_z, S_x, S_y are the spin operators. The selection rule for the spin excitations implies that they can only occur between the states differing by $m_S = \pm 1$. For $S = 1$ spin-state, we would expect only one step in the absence of transverse anisotropy ($E = 0$) and at $B = 0$T. Transverse anisotropy ($E > 0$) mixes the states and therefore a second step can occur. Hence, the $\mathrm{d}I/\mathrm{d}V$ spectra on FePc on $NbSe_2$ suggest spin-state $S = 1$ with transverse anisotropy. We fitted our data using a phenomenological spin Hamiltonian[5–8]

$$H_{\text{eff}} = g\mu_B B S_\gamma + DS_z^2 + E(S_x^2 - S_y^2)$$

where g is the Landgé g factor, μ_B the Bohr magneton, and S_γ is the component of spin along the direction of the magnetic field. Using the numerical code by M. Ternes,[5] we obtain $D = 5.5$ meV, and $E = 1.4$ meV as the best fit with the experimental data. The positive value of D indicates easy plane magnetic anisotropy.

Effect of the adsorption site on the YSR states and the spin-flip excitations

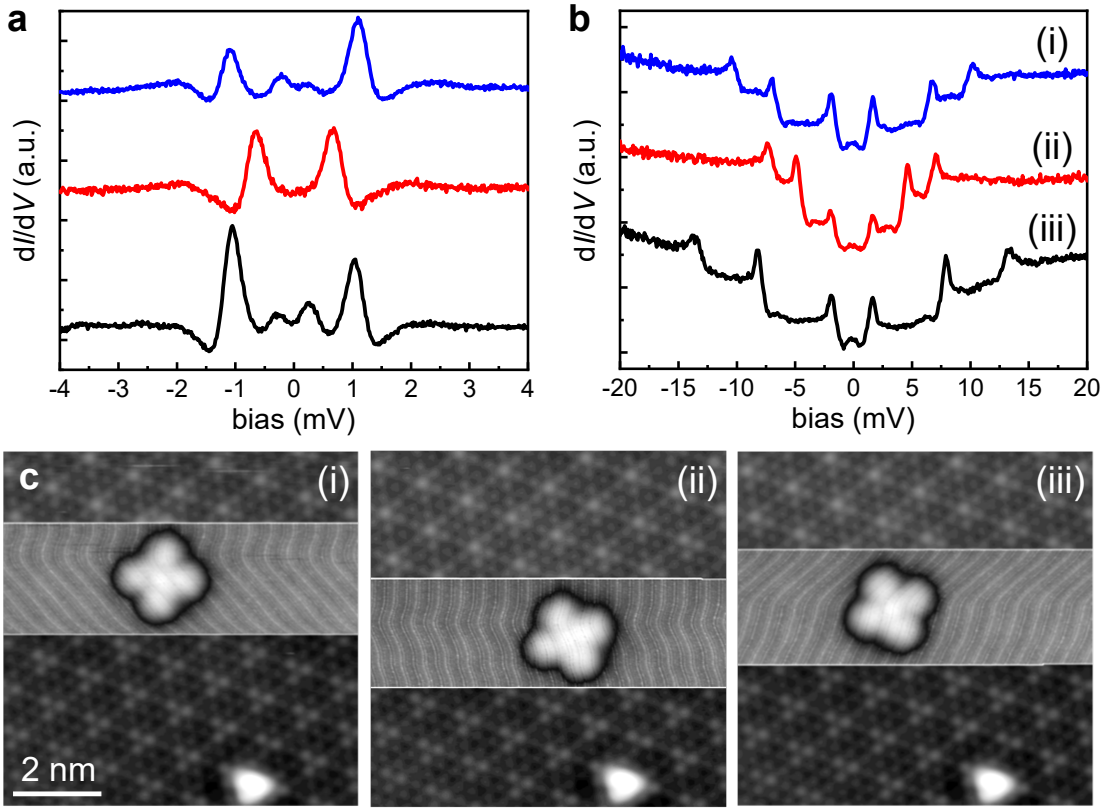

Figure S3: Effect of the adsorption site on the YSR states and the spin-flip excitations. (a) dI/dV spectra recorded on the same CoPc molecule at different adsorption sites (feedback opened at 10 mV / 1 nA; the spectra are shifted for clarity). All spectra show YSR states inside the superconducting gap. The YSR states change their excitation character between particle- or hole-like depending on the adsorption site of the CoPc molecule on $NbSe_2$, indicating different signs of the potential scattering term. (b) dI/dV spectra taken on the same FePc molecule at different adsorption sites (feedback opened at 20 mV / 1 nA; the spectra are shifted for clarity). None of the spectra show any sharp features within the superconducting gap. However, adsorption site causes variations of both E and D with typical values in the range of $1.2-2.7$ meV and $4.2-9.0$ meV, respectively. (c) Determination of the adsorption site corresponding to the three spectra shown in panel b on FePc.

Experiments on MnPc in external magnetic field

It is conceivable that there would be inelastic excitations in the energy corresponding to the features seen outside the superconducting gap on MnPc that correspond to molecular vibrations (phonons). To support our assignment of this feature to a magnetic excitation, we have carried out experiments under an external magnetic field. These experiments are difficult as they require 1) close tip-sample distances to move into the regime where we observe the spin-flip transitions and 2) we lose the enhanced energy resolution due to the superconducting tip (as superconductivity is quenched by the external field). Fig. S4a are examples of the spectra on MnPc at external fields of 5 T and 7 T (where both the substrate and the tip are normal metals). Fig. S4b,c also shows simulated spectra for $S = 3/2$ with $D = 0.6$ meV (panel b) illustrating reasonable agreement with the experiments (considering the experimental difficulties). The spin-excitation feature is weakly dependent on the magnetic field and shift towards zero bias with increasing external field strength. This also confirms that $D > 0$ (we would expect opposite and stronger magnetic field dependence for $D < 0$ as shown in Fig. S4c). The simulations were carried out using a phenomenological spin Hamiltonian[5–8] and using the numerical code by M. Ternes.[5]

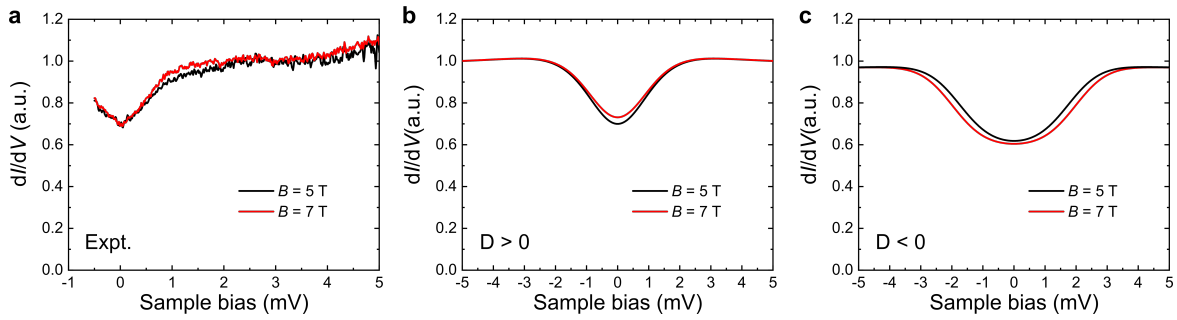

Figure S4: Spin-flip excitations in MnPc under external magnetic field. (a) Experimental results on a MnPc molecule on $NbSe_2$ substrate under external magnetic field showing the spin-excitations. (b,c) Simulated spectra using $D = 0.6$ meV (b) and $D = -0.6$ meV (c) ($g = 2$, $T = 4.2$ K).

Numerical renormalization group calculations

The impurity model is solved using the numerical renormalization group (NRG) method.[9,10] The NRG is a numerical procedure for solving quantum impurity models that is based on a logarithmic discretization of the continuum of electrons (here itinerant electrons from the substrate hybridized with the molecular states). The discretization is controlled by the parameter $\Lambda > 1$ that determines the coarseness of the frequency grid, $\omega_n \sim \Lambda^{-n}$. The discretized Hamiltonian is transformed to a linear tight-binding representation that is diagonalized iteratively. One can compute static properties (expectation values of various operators), thermodynamics, as well as dynamic properties (spectral functions). The results, in particular spectra, can be significantly improved by performing several calculations for interleaved discretizations grids and averaging the results. This tends to remove the discretization artifacts which are periodic functions in $\ln \omega$ with period $\sqrt{\Lambda}$; using $N_z = 2^k$ grids leads to a good cancellation of the fundamental frequency and the first $k-1$ harmonics.

In this work, the calculations have been performed with the "NRG Ljubljana" implementation of the technique. We used $\Lambda = 2$, $N_z = 16$, and kept up to 12000 states/multiplets (or states with energies up to $10\omega_N$, with ω_N the characteristic energy scale at the N-th step of the iteration). The conduction band was assumed to have a constant density of states $\rho = 1/(2\mathcal{D})$ ranging in energy from $-\mathcal{D}$ to $\mathcal{D}$; $\mathcal{D}$ also serves as the energy unit. The gap is fixed at $\Delta = 10^{-3}\mathcal{D}$ unless otherwise specified. The spectra were computed using the density-matrix NRG algorithm.[11]

The energies of the sub-gap states can be directly extracted from the renormalization-group flow diagrams in the NRG. This approach is significantly more accurate than determining the peak positions in the spectra, and does not suffer from any broadening artifacts. Example results are shown in Fig. S5

The positions of the spin-flip excitation energies can be determined from the spectral function, for instance by locating the peak position or the inflection point that approximately corresponds to the center of the step. Due to strongly changing line-shape of the

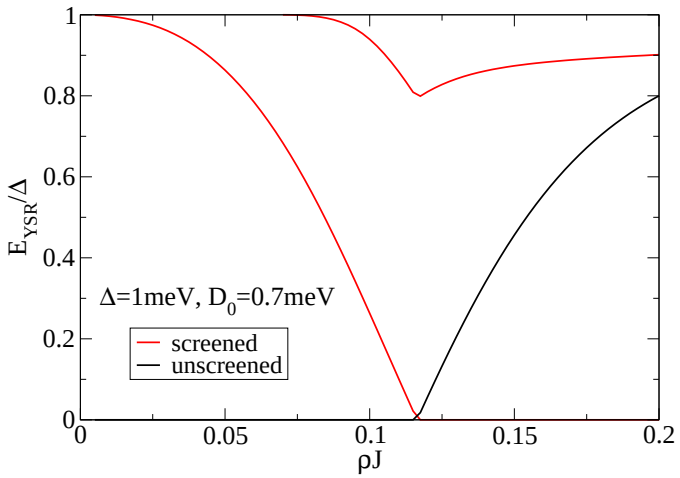

Figure S5: Energies of the many-body states, referenced to the ground-state energy of the system. This diagram shows the energies of all states below the edge of the continuum excitations. The lowest state is hence by definition the ground state, while the excited states give rise to the YSR peaks in the spectra. Black lines correspond to the states resulting from the $S = 3/2$ multiplet after anisotropy splitting (i.e., the $S_z = \pm 1/2$ pair). Red lines correspond to the states resulting from the impurity state "screened" by binding one Bogoliubov quasiparticle from the continuum. These states originate from the $S = 1$ multiplet and are separated into a $S_z = 0$ (lower energy) and a $S_z = \pm 1$ (higher energy) subsets. The $S_z = 0$ YSR state is present for all J, the $S_z = \pm 1$ pair starts emerging from the continuum at $\rho J \approx 0.08$. At $\rho J \approx 0.12$, a quantum phase transition between the $S_z = \pm 1/2$ and $S_z = 0$ many-body states occurs.

equilibrium spectral function, this procedure is somewhat ill-defined, and furthermore suffers from possible broadening artifacts. In theoretical calculation using the NRG one can, however, use a more robust and direct approach for very accurately extracting the energies of spin excitations. It consists of computing the transverse part of the dynamical spin susceptibility function

$$\chi_\perp(\omega) = \langle\langle S^x; S^x \rangle\rangle_\omega. \tag{1}$$

The spin excitation energies can then be directly read off from the peak position, which is unique and very well defined. This is illustrated in Fig. S6

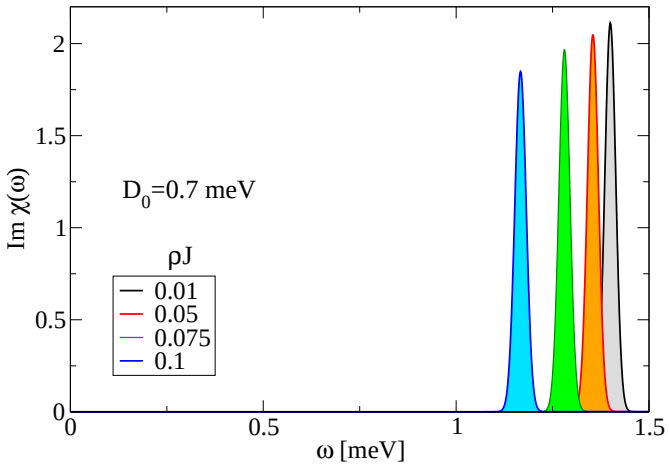

Figure S6: Dynamical spin susceptibility for a range of exchange couplings J. Here we plot the imaginary part of the transverse component of the dynamical spin susceptibility which quantifies the spin-flip transitions of the system. The peak position corresponds to $\omega_{\mathrm{sf}} = 2D_{\mathrm{eff}}$, i.e., the renormalized spin-flip energy. The peak-width is related to the life-time of the spin excitations, but here it is overbroadened for numerical reasons.

Properties of the anisotropic $S = 3/2$ Kondo model

The spectral functions for a range of values of the exchange coupling for $S = 3/2$ are shown in Fig. S7 (with parameter values corresponding to the experiments on MnPc).

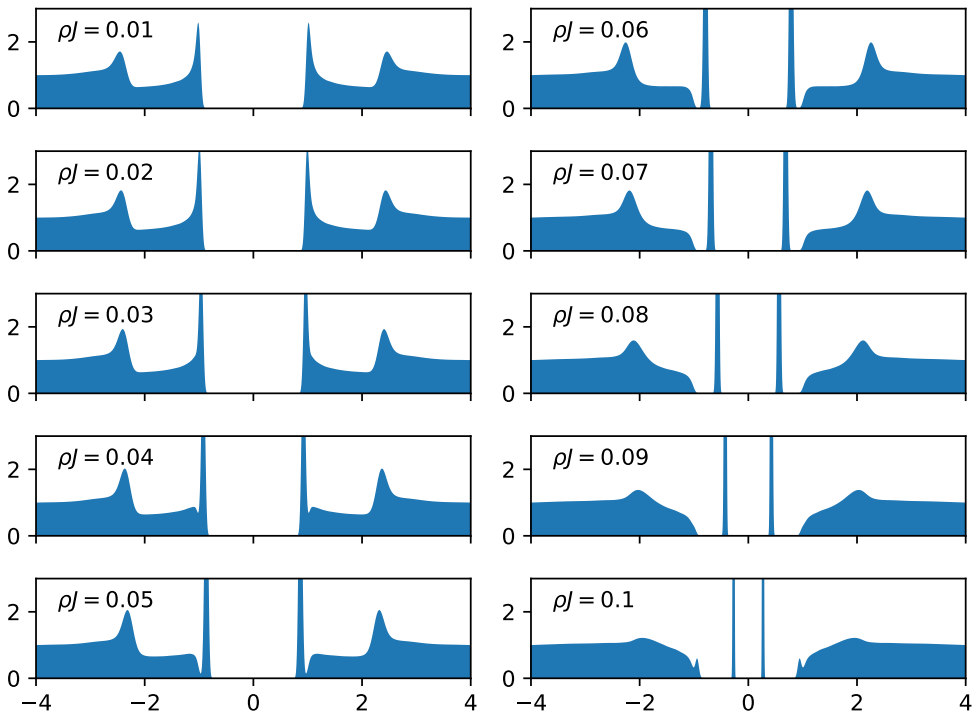

Figure S7: Spectral functions for a range of exchange coupling strengths. These plots correspond to horizontal line-cuts of the density plot in Fig. 4a of the main text. They show more clearly how the YSR state detaches from the band edge of the continuum of Bogoliubov excitations, and how the spin-flip line-shape evolves (in particular for $\rho J \geq 0.06$, i.e., after the emergence of YSR as a well-defined sub-gap state). At $\rho J \sim 0.1$, a new sub-gap feature starts to detach from the band edge: this is an additional YSR state (of type $|S_z = 1\rangle \pm |S_z = -1\rangle$) that results from the magnetic anisotropy splitting of the $S = 1$ YSR multiplet. This parameter range is, however, not experimentally relevant.

The insensitivity of the YSR state energy on D_0 is illustrated in Fig. S8, which enables us to calibrate the exchange coupling based on the experimental YSR energies.

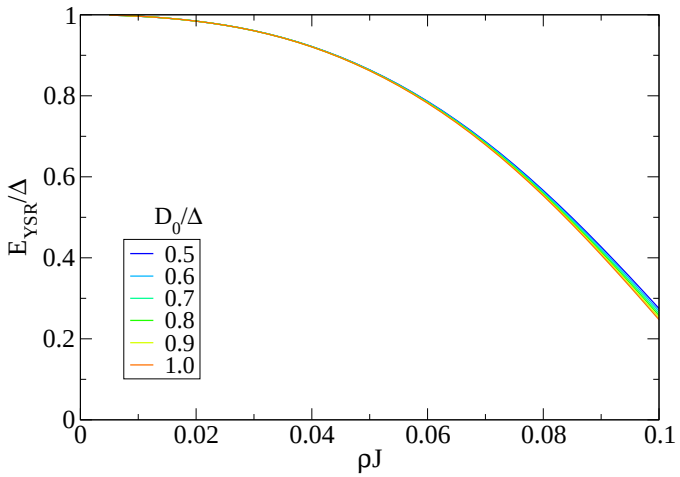

Figure S8: Yu-Shiba-Rusinov state energy as a function of exchange J for $S = 3/2$ model. The results are extracted from the highly-accurate NRG renormalization flow diagrams. The weak dependence on the value of the bare magnetic anisotropy D_0 enables the use of these results as a calibration of the tip offset above MnPc in terms of the exchange coupling J even in the absence of prior knowledge of the precise value of (bare) anisotropy.

Bare magnetic anisotropy D_0 as a function of the tip-sample distance

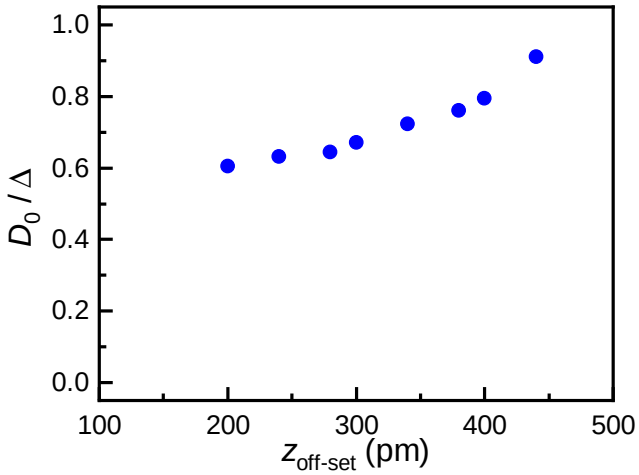

Figure S9: Bare magnetic anisotropy D_0. These values are extracted from the experimental D_{eff}/Δ values by subtracting the theoretically predicted ρJ dependence and plotted here as a function of the tip-sample distance offset.

Comparison of the spectral function with normal metal and superconducting substrate

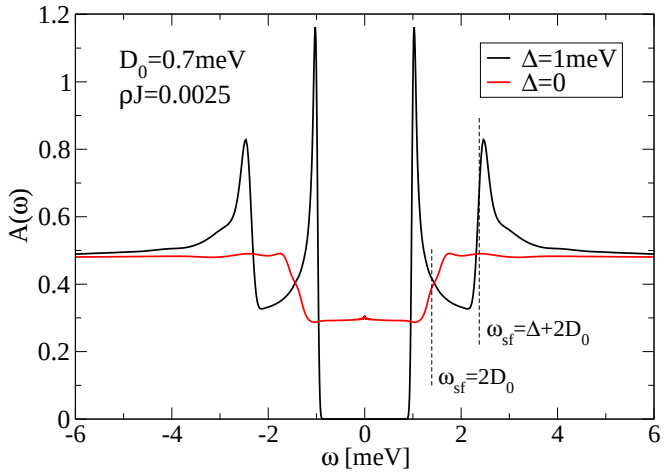

Figure S10: Calculated impurity spectral function for normal-state and superconducting substrate. We compare the low-energy parts of the spectral functions computed for an anisotropic Kondo impurity model ($S = 3/2$, longitudinal anisotropy D_0) in the limit of very small exchange coupling J, so that the Kondo temperature is negligibly small. For normal-state substrate, the spectrum shows steps due to inelastic excitations for bias voltage beyond the spin-flip excitation threshold $\omega_{\rm sf} = 2D_0$. The significant width of the step is a broadening artifact of the numerical method (lower broadening parameter would lead to stronger artifacts, which are already visible in these results in the form of weak oscillatory features). For superconducting substrate, a gap is formed, while the spin-flip features are shifted to $\omega_{\rm sf} = \Delta + 2D_0$. Furthermore, the spectral shape of the inelastic excitations inherits the form of the density of states of the superconductor near the threshold of the band of Bogoliubov excitations.

Extraction of inelastic-excitation step heights

Extracting the amplitude of the inelastic excitations in the case of a normal-state substrate is simple: extract the step amplitude and reference it to the asymptotic value. For a superconducting substrate, the inelastic excitation corresponds to a spectral feature with a complicated shape that also changes with the increasing value of the exchange coupling.

In order to compare these results with the experiments, we have used two different approaches to extract the amplitude from computed spectral functions. For low J (up to $\rho J \approx 0.06$), one can define the height as the difference between the minimum value of LDOS (this point occurs between the edge of the gap and the spin-flip resonance peak) and the asymptotic value. For larger J, this minimum no longer exists. Instead, a plateau-like structure exists for J up to $\rho J \approx 0.09$. In this range, one can define the amplitude as the difference between the value at the center of this plateau and the asymptotic value. Finally, for large J, no meaningful definition exists.

The maximum of the spectral function at the position of the spin excitation does not provide information about the amplitude of the spin-flip excitation, but rather reflects the properties of the bottom edge of the continuum (i.e., for small J, information about the superconducting coherence peak in the impurity spectral function).

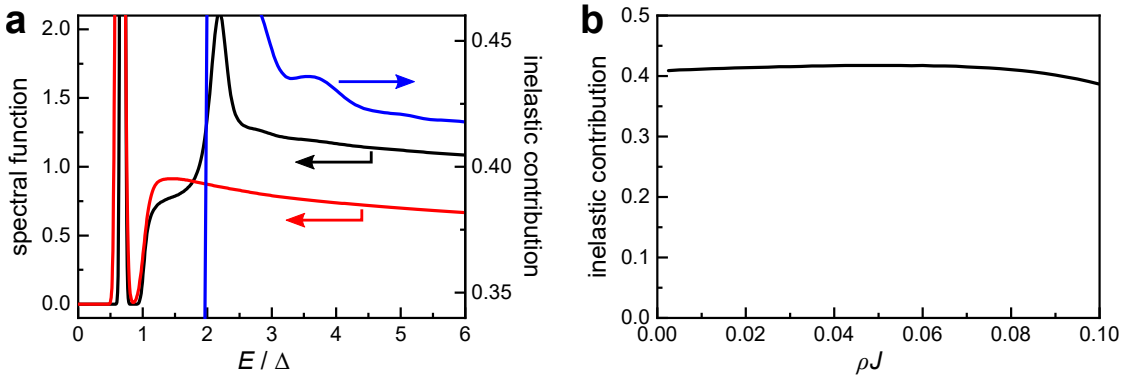

Figure S11: Estimating the real inelastic contribution to the total spectral function. (a) Calculated spectral functions with $\rho J = 0.07$ and $D_0 = 0.7$ meV (black line) or $D_0 = 5.0$ meV (red line). The difference is given by the blue line. (b) The asymptotic value of the inelastic contribution as a function ρJ for $D_0 = 0.7$ meV.

The procedure above yields the results shown in Fig. 4e of the main manuscript and corresponds physically to the visibility of the inelastic features. It is in spirit similar to how the spin-flip amplitude can be (and was) estimated experimentally. On the other hand, the true inelastic contribution to the total spectral function can be assessed by comparing the calculated response to that obtained with the same ρJ and large value of D_0. Example of such curves (at $\rho J = 0.07$) is shown in Fig. S11a. This plot shows the calculated response with $D_0 = 0.7$ meV (black line) and with $D_0 = 5$ meV (red line). The asymptotic value of their difference (blue line) gives direct access to the inelastic contribution to the total spectral function. This is plotted as a function of ρJ in Fig. S11b showing values very close to the expected magnitude of 0.4 for pure spin-flip excitations on a normal metal substrate.

Properties of the anisotropic $S = 1$ Kondo model

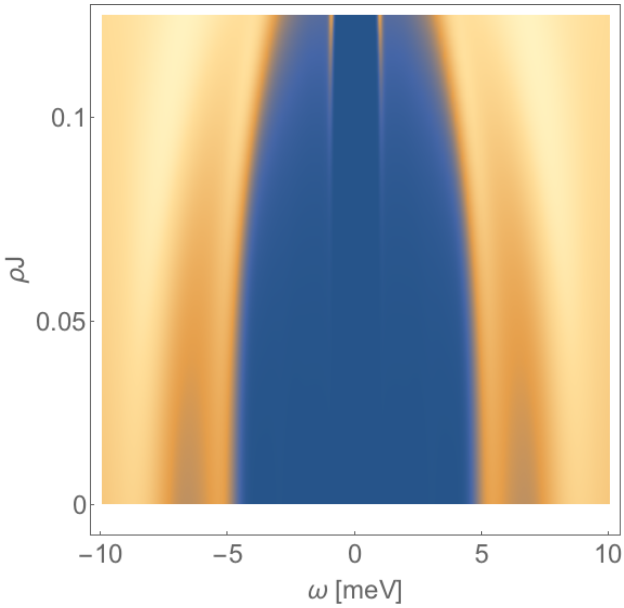

Figure S12: Theoretical spectral functions for a $S = 1$ impurity with varying exchange coupling J. Spectral function for the anisotropic $S = 1$ Kondo impurity with magnetic anisotropy parameters $D = 5.5\,\text{meV}$ and $E = 1.5\,\text{meV}$ (spin-flip excitation energies $D - E = 4\,\text{meV}$ and $D + E = 7\,\text{meV}$). At low J, the superconducting band edges are hardly visible, but their amplitude increases with increasing J. At still higher J (not shown here), a $S = 1/2$ sub-gap YSR state detaches from the gap edge.

References

(1) Blum, V.; Gehrke, R.; Hanke, F.; Havu, P.; Havu, V.; Ren, X.; Reuter, K.; Scheffler, M. Ab Initio Molecular Simulations with Numeric Atom-Centered Orbitals. *Comput. Phys. Commun.* **2009**, *180*, 2175 – 2196.

(2) Havu, V.; Blum, V.; Havu, P.; Scheffler, M. Efficient Integration for All-Electron Electronic Structure Calculation Using Numeric Basis Functions. *J. Comput. Phys.* **2009**, *228*, 8367 – 8379.

(3) Perdew, J. P.; Burke, K.; Ernzerhof, M. Generalized Gradient Approximation Made Simple. *Phys. Rev. Lett.* **1996**, *77*, 3865–3868.

(4) Tkatchenko, A.; Scheffler, M. Accurate Molecular van der Waals Interactions From Ground-State Electron Density and Free-Atom Reference Data. *Phys. Rev. Lett.* **2009**, *102*, 073005.

(5) Ternes, M. Spin Excitations and Correlations in Scanning Tunneling Spectroscopy. *New J. Phys.* **2015**, *17*, 063016.

(6) Heinrich, A. J.; Gupta, J. A.; Lutz, C. P.; Eigler, D. M. Single-Atom Spin-Flip Spectroscopy. *Science* **2004**, *306*, 466.

(7) Hirjibehedin, C. F.; Lin, C.-Y.; Otte, A. F.; Ternes, M.; Lutz, C. P.; Jones, B. A.; Heinrich, A. J. Large Magnetic Anisotropy of a Single Atomic Spin Embedded in a Surface Molecular Network. *Science* **2007**, *317*, 1199.

(8) Ternes, M. Probing Magnetic Excitations and Correlations in Single and Coupled Spin Systems with Scanning Tunneling Spectroscopy. *Prog. Surf. Sci.* **2017**, *92*, 83 – 115.

(9) Wilson, K. G. The Renormalization Group: Critical Phenomena and the Kondo Problem. *Rev. Mod. Phys.* **1975**, *47*, 773–840.

(10) Bulla, R.; Costi, T. A.; Pruschke, T. Numerical Renormalization Group Method for Quantum Impurity Systems. *Rev. Mod. Phys.* **2008**, *80*, 395–450.

(11) Hofstetter, W. Generalized Numerical Renormalization Group for Dynamical Quantities. *Phys. Rev. Lett.* **2000**, *85*, 1508–1511.